Available online at www.sciencedirect.com

jmr&t Journal of Materials Research and Technology

www.jmrt.com.br

Original Article

Adiabatic shear band localization in an Al–Zn–Mg–Cu alloy under high strain rate compression

Muhammad Abubaker Khan[a], *Yangwei Wang*[a,b,*], *Ghulam Yasin*[c], *Faisal Nazeer*[a], *Abdul Malik*[a], *Tahir Ahmad*[d], *Waheed Qamar Khan*[e], *Tuan Anh Nguyen*[f], *Hao Zhang*[g], *Mohamed A. Afifi*[h]

[a] *School of Materials Science and Engineering, Beijing Institute of Technology, Beijing 100081, China*
[b] *National Key Laboratory of Science and Technology on Material Under Shock and Impact, Beijing 100081, China*
[c] *State Key Laboratory of Chemical Resource Engineering, College of Materials Science and Engineering, Beijing University of Chemical Technology, Beijing, 100029, China*
[d] *College of Engineering and Emerging Technologies, University of Punjab, Lahore, Pakistan*
[e] *Institute of Advanced Materials, Bahauddin Zakariya University, 60800, Multan, Pakistan*
[f] *Institute for Tropical Technology, Vietnam Academy of Science and Technology, Hanoi, Viet Nam*
[g] *Jiangsu Haoran Spray Forming Alloy Co., Ltd, China*
[h] *BCAST, Brunel University London, Uxbridge, UB8 3PH, UK*

ARTICLE INFO

Article history:
Received 13 January 2020
Accepted 6 February 2020
Available online 20 February 2020

Keywords:
Adiabatic shear bands
Al–Zn–Mg–Cu alloy
High strain rate
Precipitates

ABSTRACT

An investigation was conducted to study the effect of high strain rate compression on the microstructure and mechanical properties of a spray deposited and hot formed by forging and extrusion followed by T74 (393 K/8h + 433 K/24 h) heat treatment Al–Zn–Mg–Cu alloy. The results show that the strength of the Al alloy is increased with increasing strain rate from $1.0 \times 10^{-3}\ s^{-1}$ to $5.0 \times 10^{3}\ s^{-1}$ assisted by the strain hardening rate effect. Typical adiabatic shear bands area is found in the Al–Zn–Mg–Cu alloy after compression at high strain rate. Grains are significantly refined within the shear bands areas to ~180 nm assisted by the dislocation accumulation combined with the temperature rise during the high strain rate compression. Precipitates are observed within the shear bands mainly of fine η' precipitates. These precipitates are close to Mg $(Zn, Cu, Al)_2$ assisted by diffusion provided by dislocations.

1. Introduction

The favourable mechanical properties, such as acceptable strength, good ductility, fracture toughness and impact resistance are all required for the structural applications

* *Corresponding author.*
E-mail: wangyangwei@bit.edu.cn (Y. Wang).
https://doi.org/10.1016/j.jmrt.2020.02.024

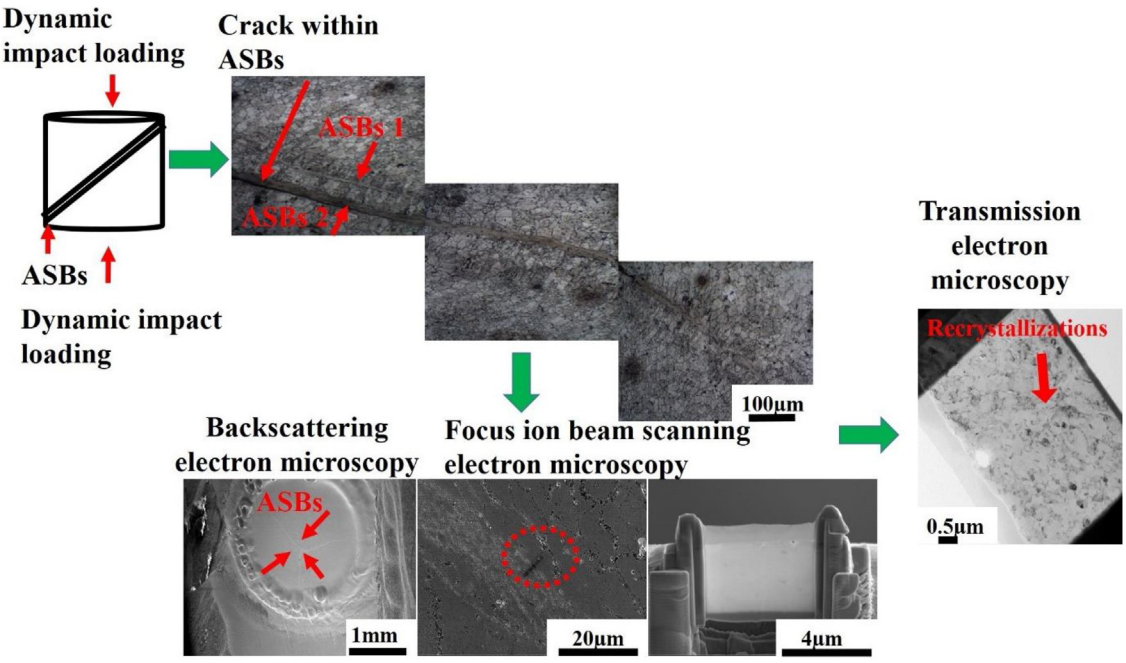

Fig. 1 – Schematic image of the ASBs area selected for the cross-sectional TEM samples with the aid of FIB sampling.

that can be subjected to different loading conditions [1–5]. Al–Zn–Mg–Cu alloys are commonly applied in aircraft components and armour automobiles owed to their outstanding mechanical properties, light weight, good impact resistance and excellent energy absorption ability [2,6]. Several reports investigated the mechanical response of Al–Zn–Mg–Cu alloys under high strain rates [7,8]. In some experimental conditions Al alloy components can be subjected to dynamic impact loading like automobiles crash which may cause failure [9]. Thus, the capability of Al–Zn–Mg alloys in withstanding impact loading is critical for the safety and reliability considerations [8–12]. Consequently, a broad understanding of the deformation of these alloys under dynamic compression is highly recommended [13].

Adiabatic shear bands (ASBs) are the areas formed due to the temperature rise and shear localization in constricted areas when subjected to high strain rates and considered as an essential failure of the materials [8]. It is found that the ASBs are initiated at areas located against the impact loading deformation [9,14]. In addition, several reports observed grain refinement and precipitates nucleation within these band areas [8,15,16]. For example, it was documented that the deformation induced dislocations and temperature rises in the Al alloy matrix during high strain impact loading promote precipitation process and phase transformation with the presence of dissolved precipitates [16,17]. Another study reported that after high strain rate compression of an Al–Zn–Mg alloy the grains are evolved to dislocation cell structures with presence of shear bands comprised of fine grains [18]. In another related studies, it was found that spray deposited Al–Zn–Mg alloys are suitable materials for the ballistic impact safety because of their higher strength and good ballistic properties [9,19].

Thus, it can summarize that recrystallization and precipitation can be presented within the ASBs areas under high strain rates impact. However, there is lack of literature about deeper analysis of precipitation with in these bands and how grains are formed after high strain rates compression. Although these data are significantly important for the practical use of these alloys. Therefore, the main objective of this study is to examine the ASBs area and precipitates within these bands after high strain rate compression of an Al–Zn–Mg–Cu alloy.

2. Experimental material and procedures

The experiments were conducted using a spray formed (SF) Al–Zn–Mg–Cu alloy brought from Haoran Spray Forming Alloy Co., Nanjing. The major alloying elements in the SF Al alloy in wt% is Al-8%, Zn-2.3%, Cu-1.7%, Mg-0.12%, and Zr-0.8%. The spray ingot is heated for 2.5 h in a furnace and then hot formed (forging and extrusion) by 703 K. More details about the hot forming process was described earlier [2]. The hot formed alloy is then treated by solution treatment at 733 K for 1.6 h followed with water quenching and further T74 heat treatment by 393 K/8h + 433 K/24 h. For quasi-static and high strain rate compression, samples are machined to ø = 5 mm × 5 mm along the extrusion direction. The quasi static tests were carried out using the electronic universal material testing machine (INSTRON 5985) at strain rate of 1.0×10^{-3} s^{-1}. The high strain rate tests were performed by using the Split Hopkinson Pressure Bar (SHPB) method at a 5.0×10^{3} s^{-1} described earlier [13]. The prescribed samples after the hot forming and the T74 heat treatment will be notified as spray formed for simplicity.

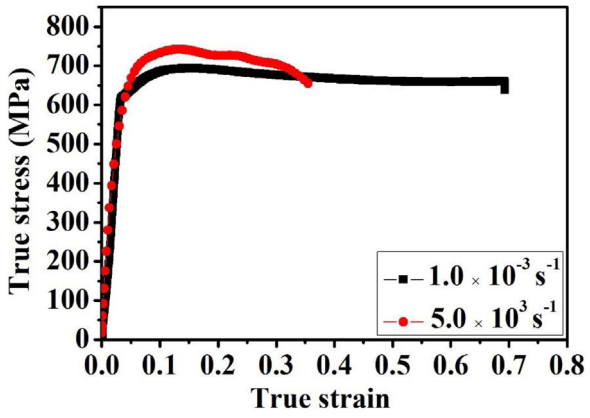

Fig. 2 – The true stress-true strain curves of Al–Zn–Mg–Cu under compression at quasi-static and high strain rates compression.

The cross-sectional transmission electron microscopy (TEM) samples from the ASBs area were cut with the aid of focused ion beam (FIB) after the compression testing by one month. The samples were carefully prepared using an FEI Helios Nano lab 600i Dual Beam FIB to produce ultra-thin samples for TEM (thickness ~50 nm) [20]. More information about the preparation of TEM specimen through FIB can be found in the previous articles [21,22]. Nano-machining of the ASB area with the aid of the dual beam FIB is illustrated in Fig. 1. The FIB prepared sample from the ASBs region was then characterized by TEM. Aberration corrected TEM (FEI Titan Themis 80–300) was used to investigate the precipitates within the ASBs. Crystallographic orientation are characterized on the FIB sample by FEI Tecnai G2 F20 S-Twin FEG electron microscopy with a precision electron diffraction (PED) control unit operating at 200 Kv [23,24].

3. Results and discussion

3.1. Dynamic mechanical properties

Fig. 2 presents the true stress-strain curves of the SF Al–Zn–Mg–Cu alloy. It is observed that the Al alloy possess higher yield and ultimate strengths after compression at $5.0 \times 10^3\ s^{-1}$ by comparison with compression at $1.0 \times 10^{-3}\ s^{-1}$ [5]. The yield strength and peak stress under $5.0 \times 10^3\ s^{-1}$ are higher by ~10 MPa over the Al alloy compressed at $1.0 \times 10^{-3}\ s^{-1}$.

The deformation mechanism of the metallic material is controlled through the internal structure of the material and the strain hardening rate. The strength of the SF Al alloy increases with increasing the strain rate by following [25]:

$$\sigma = k\dot{\varepsilon}^m \tag{1}$$

Where σ is the flow stress, k is a parameter that depends upon structure of the material and temperature and m is the strain rate sensitivity (SRS) parameter. According to Refs. [5,26], the SRS is depending on the properties of the Al–Zn–Mg–Cu alloy after the T74 heat treatment leading to the increased strength after compression at high strain rates.

3.2. Microstructure investigation before and after compression

The microstructure of the SF Al–Zn–Mg alloy was studied and characterized in an earlier report [2]. The grain size of the SF alloy was ~35–40 μm including homogeneously distributed fine precipitates. Precipitates are predominantly of G.P. zones and η' particles with average size ~15 nm. Typical bright field (BF) and dark field (DF) TEM micrographs of the SF Al alloy after compression at $5.0 \times 10^3\ s^{-1}$ are displayed in Fig. 3. Recrystallized and elongated grains are observed within the ASBs in Fig. 3(a) and (b). In addition, several very fine recrystallized grains are also observed in Fig. 3(c) with the presence of some dislocation tangles inside the sub grains. The presence of some coarse precipitates close to dislocations can be owed to the dynamic precipitation during compression [27] as depicted in Fig. 3(d). Precipitates are mainly of η' phase as verified by the selected area diffraction (SAED) pattern shown in Fig. 3(e).

Aberration-corrected TEM images of a selected ASBs area are illustrated in Fig. 4. Fig. 4(a) shows large number of homogeneously distributed precipitates which are spherical and platelets morphologies with size range of ~9–14 nm. Fig. 4(b) shows a high magnification TEM presenting very fine precipitates which are distributed within the grain.

3.3. Microstructure evolution within the ASBs area

Typical TEM images with PED are displayed in Fig. 5. It is apparent from Fig. 5(a) that grains in the ASBs area are refined to ~180 nm. This owes to the high temperature and high shear strain assisted by the high deformation rate within the ASBs leading to dynamic recrystallization [28]. The presence of few coarse elongated grains can be resulted from the inhomogeneous heat distribution during compression [16]. The temperature within the ASBs can be estimated as follows [28,29]:

$$T - T_{\circ} = \beta/\rho c \int_0^{\varepsilon f} \sigma d\varepsilon \tag{2}$$

where Tis the temperatures of samples during compression and $T_{\circ}$is the room temperature, β is the coefficient of thermal transition ($\beta \sim 0.9$) [28], $\rho$is the density of Al alloy ($\rho = 2.85\ g/cm^3$), cis the heat coefficient, ($c = 860\ j/kg$), $\varepsilon f$is the true strain and $d\varepsilon$is change in strain [30]. The shear strain within the adiabatic shear band area is determined by tilting the angle θ between the orientations of the extruded grains and the ASBs by using Wright criterion [31] as follows:

$$\varepsilon_s = tan\theta \tag{3}$$

Where ε_s is the change in strain inside the adiabatic shear band, θ is the angle between adiabatic shear band and grains orientation [28]. By substituting Eq. (3) in Eq. (2), the value of temperature inside the ASBs can be estimated as ~410 °C. This temperature is enough for dynamic recrystallization within

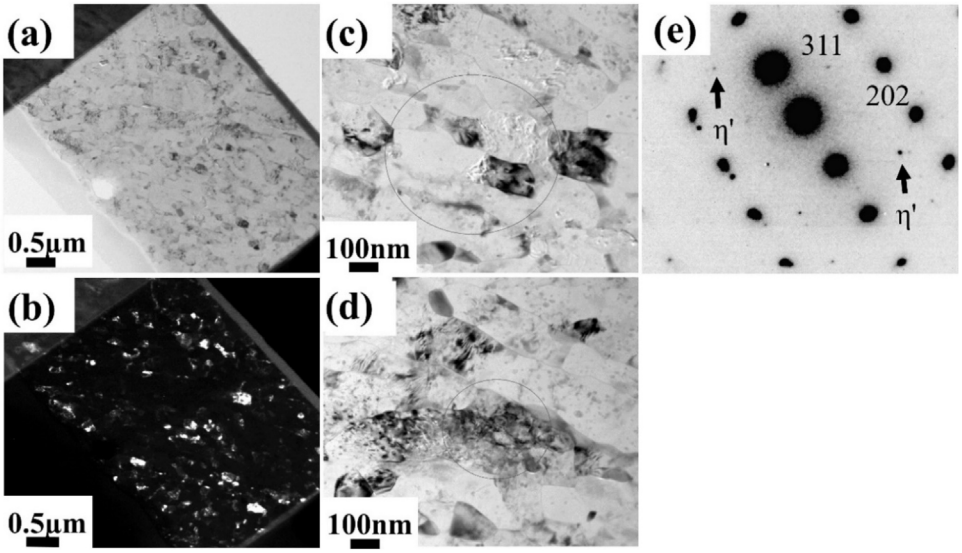

Fig. 3 – The ASBs areas after high strain rate compression of Al–Zn–Mg–Cu alloy under 5.0 × 10^3 s^{-1}: (a) low magnification of BF TEM and (b) low magnification of DF TEM, (c) BF TEM in high magnification showing equiaxed fine grains, (d) BF TEM in high magnification showing subgrains with dislocation tangles and (e) SAED pattern along <112>$_{Al}$ of selected area identified in (d).

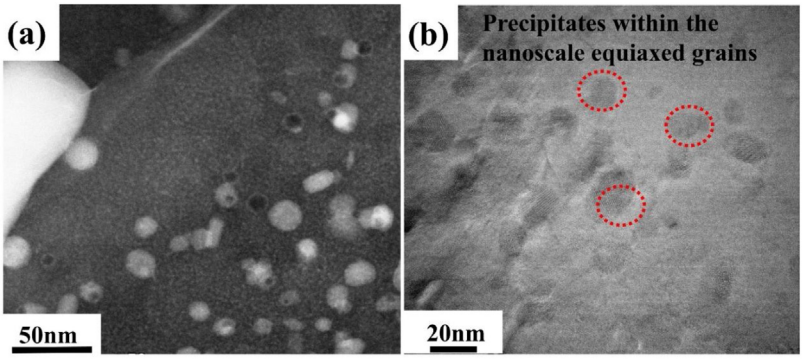

Fig. 4 – ASB area after compression at high strain rates (a) DF TEM at low magnification and (b) BF TEM images at high magnification.

the ASBs [16,31]. Fig. 5(b) shows the texture within the shear band area which is mainly of Goss and annealing textures. The high intensity texture of 7.6 can be resulted from the recrystallization during compression [32]. Grains are mainly of high angle grain boundaries as depicted in Fig. 5(c) [33]. High angle grain boundaries (HAGBs) ~46.5% are identified by red color in Fig. 5 (a), while low angle grain boundaries (LAGBs) ~40.3 % are identified in black color.

3.4. *EDX mapping inside the shear band*

Fig. 6(a) shows high-angle annular dark-field scanning transmission electron microscopy (HAADF-STEM) image of homogeneously distributed precipitates observed after high strain rate compression of the SF Al alloy. Fig. 6(b) presents the energy dispersive X-ray microanalysis (EDX) line scan of selected fine precipitates. Fig. 6(c) and (d) display the EDX mapping where precipitates are rich with Mg, Zn and Cu. According to the EDX line scan the first precipitate in the left is η as Mg:Zn is 2:1 while the other 2 are η' precipitates making Mg:Zn close to 1 [34,35].

Fig. 7 shows HAADF-STEM and EDX mapping of a selected precipitate after high strain rate compression observed close to the grain boundaries. Fig. 7(a) presents the precipitates which has platelet morphology and the EDX line scan. By inspection of Fig. 7(b), the precipitate comprises Zn, Mg, and Cu. It is recommended that the precipitate is also η' phase by assessment the Mg:Zn ratio using EDX [36].

Furthermore, the observed precipitates within the ASBs contain a significant proportion of Zn, Mg and Cu in Figs. 6 and 7. These precipitates had a stoichiometry close to $MgZn_2$ and Mg $(Zn, Cu, Al)_2$, which is defined as η' particle [34,35]. Prior reports [34] recommended that Zn atoms present in $MgZn_2$ could substituted through Cu and Al atoms. It was determined that in the quaternary Al–Zn–Mg–Cu system, $MgZn_2$ and AlMgCu phases build an isomorphous series by Al and Cu solute particles replacing for Zn in $MgZn_2$ assisted by dislocation motion [37]. This shows that the region around

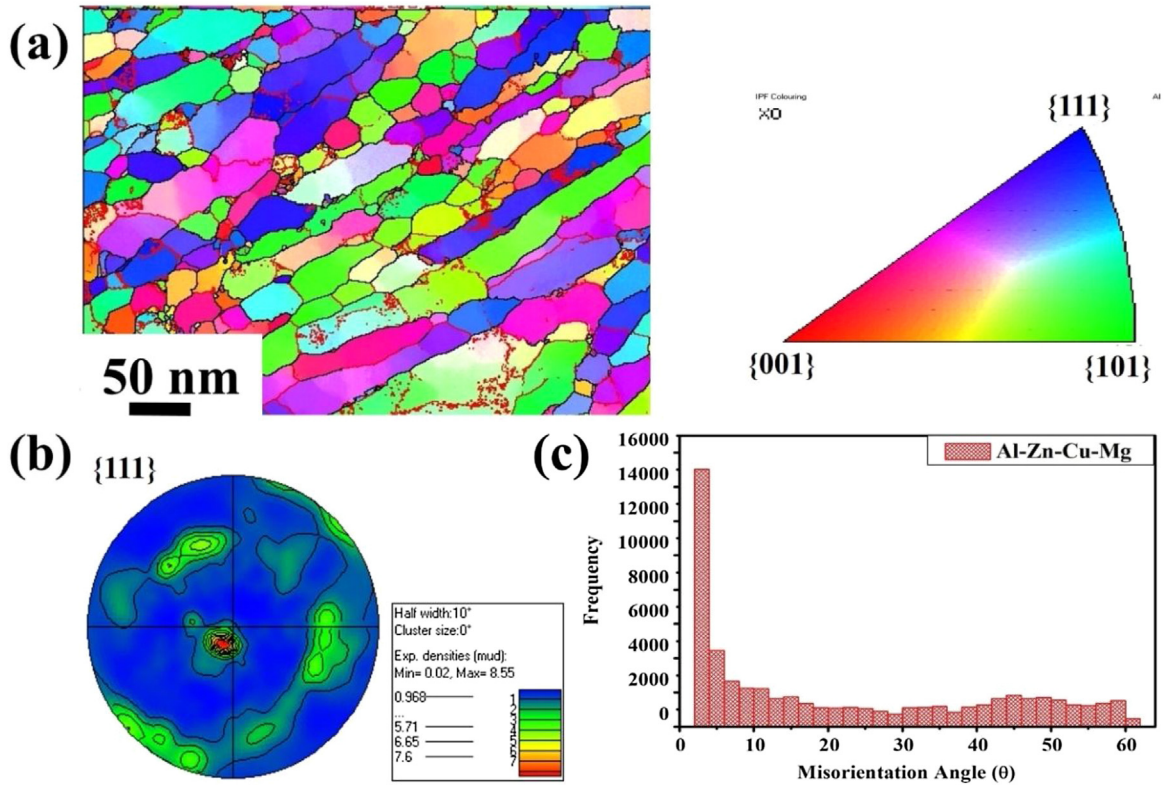

Fig. 5 – (a) Showing the PED analysis inside the shear band region of Al–Zn–Mg–Cu alloy under 5.0 × 10^3 s^{-1} represents the fine and elongated grains, (b) the texture analysis of shear band region and (c) the misorientation grain boundary distribution.

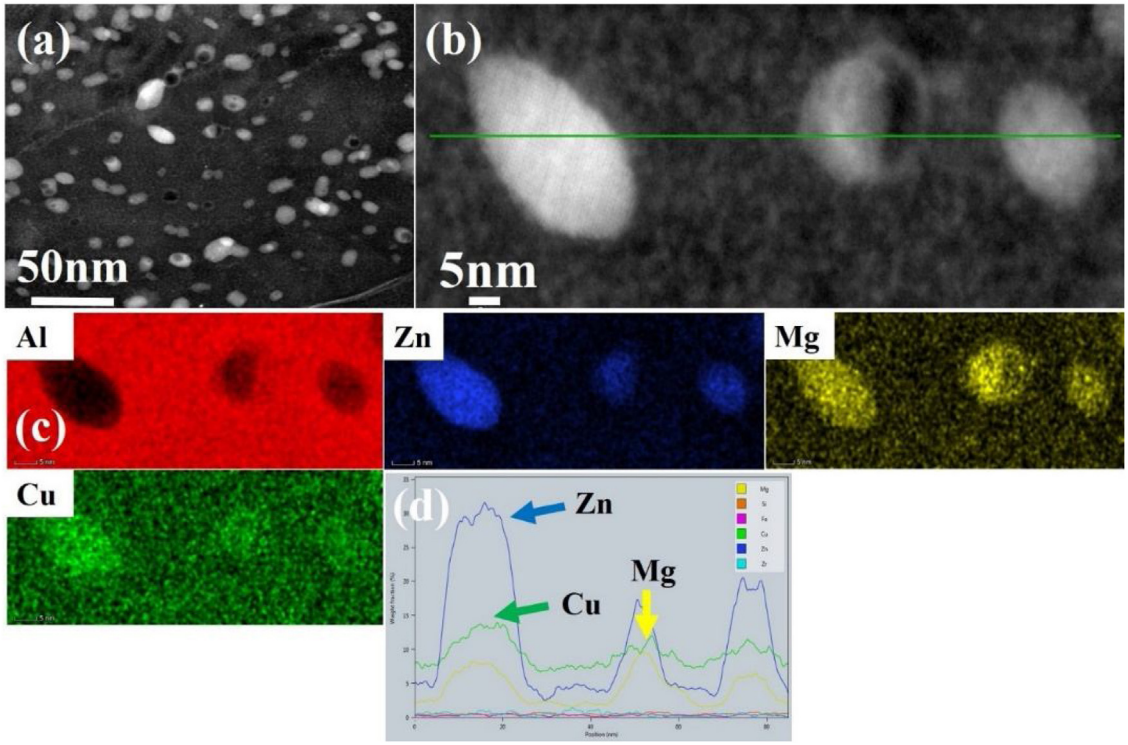

Fig. 6 – (a) HAADF-STEM micrographs of fine precipitates inside the elongated grains within the ASBs after compression at 5.0 × 10^3 s^{-1} (b) EDX-line scan of the selected precipitate area (c) EDX mapping and (d) the corresponding composition peaks.

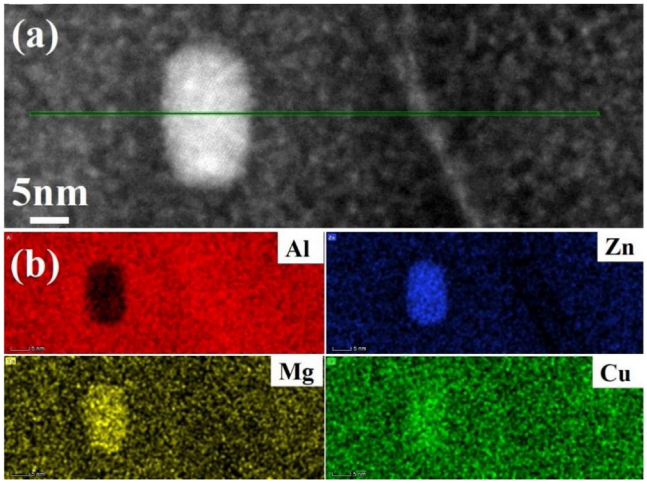

Fig. 7 – (a) HAADF-STEM and (b) EDX mapping of ASBs after compression at 5.0 × 10^3 s^{-1} within the ASB area after high strain rate compression.

the $MgZn_2$ became rich with Cu [38]. Thus, Al–Zn–Mg alloy system η' precipitates can have a composition of $Mg(Zn, Cu, Al)_2$ under high strain rates by substituting Zn atoms in $MgZn_2$ by Cu and Al assisted by diffusion from dislocation motions [38,39]. Large amount of precipitates were detected within the ASBs area although it was mentioned that the temperature can reach to ~410 °C in this area during compression. This can be owed to the effect of natural aging in this area which enhanced the precipitation process. In addition, the presence of large amount of dislocations in the ASBs area depicted in Fig. 3 assists the precipitates formation during the natural aging processes. Although several studies [16,40] mentioned that the high temperature inside the shear bands can lead to the dissolving of the precipitates after compression. Natural aging can be effective in this area by diffusion of solutes assisted by the large amount of dislocations in the band region [41,42].

4. Conclusions

The microstructure characteristic and precipitates evolution within the ASBs of SF Al–Zn–Mg–Cu alloys under dynamic compression has been explored. The following conclusions are:

1 The strength of the material is increased with increasing strain rate from 1.0 × 10^{-3} s^{-1} to 5.0 × 10^3 s^{-1} assisted by the strain hardening rate effect in the Al alloys. The grains are reduced to ~180 nm inside the ASBs.
2 The fine grains within the ASBs are evident with strong texture and HAGB's ~46.5%. Refined grains owed to dynamic recrystallization by shear localization of dislocation tangles within the grains and the temperature rise in the narrow shear region.
3 The homogeneous distribution of precipitates is mainly of η'-phase after high strain rate compression within the ASB area. Observed η' and η precipitates are rich in Cu forming composition of $Mg (Zn, Cu, Al)_2$ influenced by dislocation motion during high strain rate compression within the ASBs area. Although the temperature is high inside the shear bands area the presence of fine precipitates within these regions can form from the natural aging effect.

Conflict of interest

The authors declare no conflict of interest.

Acknowledgment

This project is financially supported by the National Key Laboratory Foundation of China. (Grant No. 51702015)

REFERENCES

[1] Ritchie RO. The conflicts between strength and toughness. Nat Mater 2011;10(11):817.
[2] Khan MA, Wang Y, Afifi MA, Malik A, Nazeer F, Yasin G, et al. Microstructure and mechanical properties of an Al-Zn-Cu-Mg alloy processed by hot forming processes followed by heat treatments. Mater Charact 2019;157:109901.
[3] Meyers MA, Chawla KK. Mechanical behavior of materials. Cambridge University Press; 2008.
[4] Khan MA, Wang Y, Yasin G, Malik A, Nazeer F, Khan WQ, et al. Microstructure characteristic of spray formed 7055 Al alloy subjected to ballistic impact by two different steel core projectiles impact. J Mater Res Technol 2019;8(6):6177–90.
[5] Afifi MA, Wang YC, Cheng X, Li S, Langdon TG. Strain rate dependence of compressive behavior in an Al-Zn-Mg alloy processed by ECAP. J Alloys Compd 2019;791:1079–87.
[6] Mondal C, Mishra B, Jena PK, Siva Kumar K, Bhat TB. Effect of heat treatment on the behavior of an AA7055 aluminum alloy during ballistic impact. Int J Impact Eng 2011;38(8):745–54.
[7] Yang Q, Deng Z, Zhang Z, Liu Q, Jia Z, Huang G. Effects of strain rate on flow stress behavior and dynamic recrystallization mechanism of Al-Zn-Mg-Cu aluminum alloy during hot deformation. Mater Sci Eng A 2016;662:204–13.
[8] Wu X, Li L, Liu W, Li S, Zhang L, He H. Development of adiabatic shearing bands in 7003-T4 aluminum alloy under high strain rate impacting. Mater Sci Eng A 2018;732:91–8.
[9] Zhang W, Chen X, Zhuo B, Li P, He L. Effect of strain rate and temperature on dynamic mechanical behavior and microstructure evolution of ultra-high strength aluminum alloy. Mater Sci Eng A 2018;730:336–44.
[10] Khan MA, Wang Y, Malik A, Nazeer F, Yasin G, Khan WQ, et al. Microstructure characterization of 7055-T6, 6061-T6511 and 7A52-T6 Al alloys subjected to ballistic impact against heavy tungsten alloy projectile. Arch Civ Mech Eng 2019;19(4):1484–96.
[11] Lee W-S, Sue W-C, Lin C-F, Wu C-J. The strain rate and temperature dependence of the dynamic impact properties of 7075 aluminum alloy. J Mater Process Technol 2000;100(1):116–22.
[12] Afifi MA, Pereira PHR, Wang YC, Wang Y, Li S, Langdon TG. Effect of ECAP processing on microstructure evolution and dynamic compressive behavior at different temperatures in an Al-Zn-Mg alloy. Mater Sci Eng A 2017;684:617–25.
[13] Mishra B, Mondal C, Goyal R, Ghosal P, Kumar KS, Madhu V. Plastic flow behavior of 7017 and 7055 aluminum alloys under different high strain rate test methods. Mater Sci Eng A 2014;612:343–53.

[14] Li Z, Zhao S, Alotaibi SM, Liu Y, Wang B, Meyers MA. Adiabatic shear localization in the CrMnFeCoNi high-entropy alloy. Acta Mater 2018;151:424–31.
[15] Meyers MA. Dynamic behavior of materials. John Wiley & Sons; 1994.
[16] He H, Wu X, Sun C, Li L. Grain structure and precipitate variations in 7003-T6 aluminum alloys associated with high strain rate deformation. Mater Sci Eng A 2019;745:429–39.
[17] Xu Y, Zhong W, Chen Y, Shen L, Liu Q, Bai Y, et al. Shear localization and recrystallization in dynamic deformation of 8090 Al–Li alloy. Mater Sci Eng A 2001;299(1–2):287–95.
[18] Xiong Y, Li N, Jiang H, Li Z, Xu Z, Liu L. Microstructural evolutions of AA7055 aluminum alloy under dynamic and quasi-static compressions. Acta Metall Sin 2014;27(2):272–8.
[19] Khan MA, Wang Y, Cheng H, Nazeer F, Yasin G, Farooq MU, et al. Ballistic behaviour of spray formed AA7055 aluminum alloy against tungsten core projectile impact. Vacuum 2019;159:482–93.
[20] Yin C-h, Liang Y-l, Liang Y, Li W, Yang M. Formation of a self-lubricating layer by oxidation and solid-state amorphization of nano-lamellar microstructures during dry sliding wear tests. Acta Mater 2019;166:208–20.
[21] Langford RM, Rogers M. In situ lift-out: steps to improve yield and a comparison with other FIB TEM sample preparation techniques. Micron 2008;39(8):1325–30.
[22] Schaffer M, Schaffer B, Ramasse Q. Sample preparation for atomic-resolution STEM at low voltages by FIB. Ultramicroscopy 2012;114:62–71.
[23] Brons JG, Thompson GB. Orientation mapping via precession-enhanced Electron diffraction and its applications in materials science. JOM 2014;66(1):165–70.
[24] Viladot D, Véron M, Gemmi M, Peiró F, Portillo J, Estradé S, et al. Orientation and phase mapping in the transmission electron microscope using precession-assisted diffraction spot recognition: state-of-the-art results. J Microsc 2013;252(1):23–34.
[25] Li B, Pan Q, Zhang Z, Li C. Characterization of flow behavior and microstructural evolution of Al–Zn–Mg–Sc–Zr alloy using processing maps. Mater Sci Eng A 2012;556:844–8.
[26] Zhang S, Hu W, Berghammer R, Gottstein G. Microstructure evolution and deformation behavior of ultrafine-grained Al–Zn–Mg alloys with fine η' precipitates. Acta Mater 2010;58(20):6695–705.
[27] Zhang Y, Jin S, Trimby PW, Liao X, Murashkin MY, Valiev RZ, et al. Dynamic precipitation, segregation and strengthening of an Al-Zn-Mg-Cu alloy (AA7075) processed by high-pressure torsion. Acta Mater 2019;162:19–32.
[28] Yang D, An Y, Cizek P, Hodgson P. Development of adiabatic shear band in cold-rolled titanium. Mater Sci Eng A 2011;528(12):3990–7.
[29] Li DH, Yang Y, Xu T, Zheng HG, Zhu QS, Zhang QM. Observation of the microstructure in the adiabatic shear band of 7075 aluminum alloy. Mater Sci Eng A 2010;527(15):3529–35.
[30] Liu S, Wang S, Ye L, Deng Y, Zhang X. Flow behavior and microstructure evolution of 7055 aluminum alloy impacted at high strain rates. Mater Sci Eng A 2016;677:203–10.
[31] Wright TW, Wright TW. The physics and mathematics of adiabatic shear bands. Cambridge University Press; 2002.
[32] Pereira PHR, Wang YC, Huang Y, Langdon TG. Influence of grain size on the flow properties of an Al-Mg-Sc alloy over seven orders of magnitude of strain rate. Mater Sci Eng A 2017;685:367–76.
[33] Randle V, Engler O. Introduction to texture analysis: macrotexture, microtexture and orientation mapping. CRC Press; 2014.
[34] Marlaud T, Deschamps A, Bley F, Lefebvre W, Baroux B. Influence of alloy composition and heat treatment on precipitate composition in Al–Zn–Mg–Cu alloys. Acta Mater 2010;58(1):248–60.
[35] Sha G, Cerezo A. Early-stage precipitation in Al–Zn–Mg–Cu alloy (7050). Acta Mater 2004;52(15):4503–16.
[36] Afifi MA, Wang YC, Pereira PHR, Huang Y, Wang Y, Cheng X, et al. Mechanical properties of an Al-Zn-Mg alloy processed by ECAP and heat treatments. J Alloys Compd 2018;769:631–9.
[37] Zhao H, De Geuser F, Kwiatkowski da Silva A, Szczepaniak A, Gault B, Ponge D, et al. Segregation assisted grain boundary precipitation in a model Al-Zn-Mg-Cu alloy. Acta Mater 2018;156:318–29.
[38] Totten GE, MacKenzie DS. Handbook of aluminum: vol. 1: physical metallurgy and processes. CRC Press; 2003.
[39] Hu T, Ma K, Topping T, Schoenung J, Lavernia E. Precipitation phenomena in an ultrafine-grained Al alloy. Acta Mater 2013;61(6):2163–78.
[40] Chen RW, Vecchio K. Microstructural characterization of shear band formation in Al-Li alloys. Le Journal de Physique IV 1994;4(C8). C8-459-C8-464.
[41] Huang Y, Robson J, Prangnell P. The formation of nanograin structures and accelerated room-temperature theta precipitation in a severely deformed Al–4 wt.% Cu alloy. Acta Mater 2010;58(5):1643–57.
[42] Zolotorevsky NY, Solonin A, Churyumov AY, Zolotorevsky V. Study of work hardening of quenched and naturally aged Al–Mg and Al–Cu alloys. Mater Sci Eng A 2009;502(1–2):111–7.